# Compensation of Current Transformers' Nonlinearities by Tensor Linearization

Adam J. Collin, *Member, IEEE*, Antonio Delle Femine, *Member, IEEE*, Daniele Gallo, *Member, IEEE*, Roberto Langella, *Senior Member, IEEE*, and Mario Luiso, *Member, IEEE*

***Abstract*— With the proliferation of harmonic sources in power systems, current transformers (CTs), which are the most widely used current transducers in power systems, will have to measure and monitor signals with increasing levels of distortion. The accuracy of the measurement can be affected by the nonlinear response of the CT, which is dependent on the distortion in the measured signal, but nonlinear mathematical models can be used to compensate the measured value. In this paper, the complex ratio of the CT is modeled using a frequency domain model based on tensor linearization, obtaining a real-valued compensation matrix. An accurate measurement setup has been built to characterize the CTs performance in distorted conditions. Experimental results using the proposed compensation technique are presented and discussed for two commercial CTs of accuracy class 0.5 and 1. It is demonstrated that the proposed technique can accurately reconstruct the harmonic components (up to several kilohertz) of the CT primary current from the measured CT distorted secondary current.**

***Index Terms*— Current transformer (CT), frequency coupling matrix (FCM), harmonics, nonlinearity compensation, phase-dependent characteristics, power quality, power system measurements.**

## I. Introduction

THE measurement of harmonics and power quality, in general, is an essential task, particularly in the new context of smart grids with a high penetration of nonlinear loads and energy production from renewable sources. Nowadays, current and voltage instrument transformers (CTs and VTs) are still the most commonly installed current and voltage transducers in power systems, at all voltage levels. As a consequence, most measuring instruments for power system applications (power/energy measurement, power quality measurement, phasor measurement unit, etc.) use CTs and VTs.

Some recent scientific literature [1]–[6] has experimentally demonstrated that even high accuracy class CTs and VTs (i.e., accuracy class better than 0.5) may suffer from nonlinearity effects. Due to these effects, the accuracy of the CT/VT is strongly dependent on the amplitude, phase angle, and the order of harmonic content of the input waveform. Therefore, the measurement of harmonics by CTs and VTs could present an accuracy which is much lower than the accuracy class of the instrument transformer used in the measurement chain. Accordingly, accurate measurement of harmonics by the CT or VT requires the use of a nonlinear mathematical (either analytic or numerical) model for the instrument transformer, which is able to accurately reconstruct the primary quantity (i.e., current for CTs and voltage for VTs) from the measured secondary quantity.

Different techniques for mathematically describing the nonlinearity of instrument transformers have been proposed in the scientific literature, e.g., [6]–[9]. These approaches are essentially based on modeling the saturation and eddy currents phenomena in transformers. However, the performances of the proposed techniques have not been verified when harmonic distortion is present in the primary quantity. Only in [6], nonsinusoidal operating conditions are accounted but the distortion introduced by the CT at the secondary is considered dependent only on the fundamental primary amplitude.

Another approach to model nonlinear devices, commonly used for power system harmonic penetration studies in the frequency domain, is the frequency coupling matrix (FCM) approach [10]–[20]. FCMs are based on the theory of small signal analysis and are used in this research to relate the generic harmonic components of the secondary current to the variations of all of the considered harmonic components of the primary current. FCMs are a powerful tool: they are able to model the nonlinearities in power system components for both traditional devices (i.e., power transformers, ac motors, cables, and so on) as well as modern devices based on power electronic technologies. FCMs can be obtained both analytically or by numerical or experimental tests.

In [21], the FCM approach was applied to model the complex ratio of a class 0.5 CT in order to compensate the nonlinearity of the CT behavior. The FCM was derived and it was shown that by inverting this matrix, the harmonic content of the primary current can be accurately identified from the measurement of the secondary current.

This paper builds on and significantly extends the initial work presented in [21] by providing: 1) further analytical details about the FCM derivation; 2) the description of the new, and much more accurate, test setup built; 3) an extension of the frequency range from 1 to 10 kHz; 4) the characterization of a new CT with lower accuracy class; 5) a new

Manuscript received November 19, 2018; revised January 24, 2019; accepted March 1, 2019. Date of publication May 13, 2019; date of current version September 13, 2019. This work received funding by: 1) the EMPIR programme co-financed by the Participating States within EURAMET and from the European Union's Horizon 2020 research and innovation programme (Grant 17IND06 Future Grid II); 2) University of Campania "Luigi Vanvitelli" (Piano Strategico VALERE—OPEN ACCESS); 3) Italian Ministry of University and Research (Grant PON03PE-00178-1). The Associate Editor coordinating the review process was Sara Sulis. *(Corresponding author: Mario Luiso.)*

The authors are with the Department of Engineering, University of Campania Luigi Vanvitelli, Aversa 81100, Italy (e-mail: adam.collin@ieee.org; antonio.dellefemine@unicampania.it; daniele.gallo@unicampania.it; roberto.langella@unicampania.it; mario.luiso@unicampania.it).

Color versions of one or more of the figures in this article are available online at http://ieeexplore.ieee.org.

Digital Object Identifier 10.1109/TIM.2019.2905908

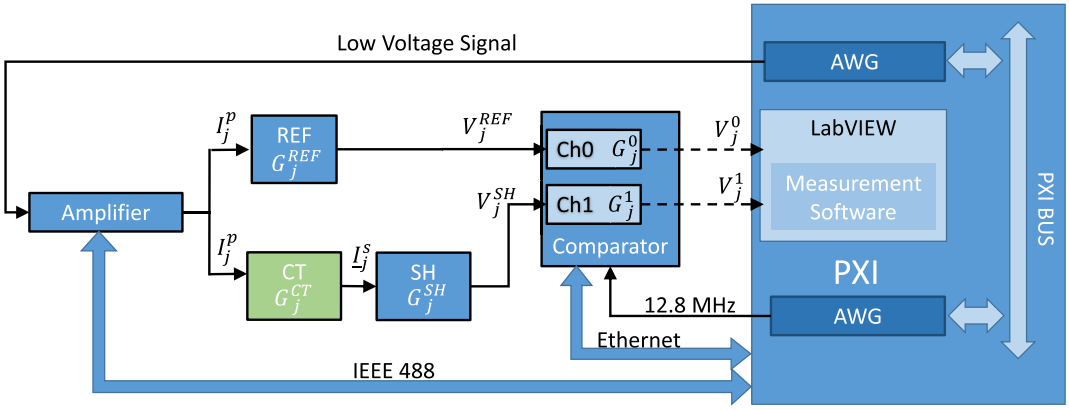


Fig. 1. Block diagram of the measurement setup for CT characterization [3].

set of experimental tests for the verification of the proposed methodology; 6) the introduction of one additional method for comparing the performance of the proposed compensation technique.

The paper is organized as follows. Section II analytically describes the proposed CT compensation technique. Section III presents the experimental setup and describes the experimental tests performed to characterize the CT. Section IV shows the derivation of the FCM of the two CTs under study. Section V discusses the use of the proposed compensation technique in a practical case comparing its performance with two other methods presented in the literature. Conclusions are given in Section VI.

## II. CT Compensation Technique

Under the hypothesis of time-periodic signals, the secondary current of a current transformer (CT) $i^s(t)$ is a function of the primary current $i^p(t)$

$$i^s(t) = g(i^p(t)) \tag{1}$$

where $g$ is a function which accounts for the nonlinearities related to the nonideal operation of the CT itself.

Under small-signal operation, any device can be linearized around proper operation base points $i_b^s(t)$ and $i_b^p(t)$. Evaluating the complex Fourier series of the quantities (italic fonts are used for complex numbers) involved gives

$$[\Delta I^s] = \left[I^s - I_b^s\right] = \boldsymbol{G}\left(\left[I^p - I_b^p\right]\right) = \boldsymbol{G}([\Delta I^p]) \tag{2}$$

where $\Delta I^s$ and $\Delta I^p$ are vectors of harmonic phasors and the function $\boldsymbol{G}$ is a complex function.

If $\boldsymbol{G}$ is linear, it may include linear cross-coupling and phase dependence between harmonics [10]. However, when linearizing general nonlinear devices, representation by a single matrix of complex numbers is not possible. The general representation is

$$\Delta I^s = \boldsymbol{G}^+ \Delta I^p + \boldsymbol{G}^- \Delta I^{p*} \tag{3}$$

where $\boldsymbol{G}^+$ and $\boldsymbol{G}^-$ are two matrices of complex numbers that couple $\Delta I^p$ and its conjugate $\Delta I^{p*}$, respectively, to give $\Delta I^s$ [18]–[21].

In real terms, $\boldsymbol{G}^+$ is able to take into account the cross coupling between primary and secondary harmonic currents, while $\boldsymbol{G}^-$ takes into account the dependence of the secondary current harmonics on the phase angle of the primary current harmonics. For example, a linear device will have a diagonal constant $\boldsymbol{G}^+$ matrix and a nil $\boldsymbol{G}^-$ matrix. These concepts will be addressed in more detail in Section IV.

Equation (3) can be elegantly and efficiently rewritten using a real-valued rank 2 tensor representation as in the following equation:

$$\begin{bmatrix} \begin{bmatrix} \Delta I^s_{2r} \\ \Delta I^s_{2i} \end{bmatrix} \\ \vdots \\ \begin{bmatrix} \Delta I^s_{Hr} \\ \Delta I^s_{Hi} \end{bmatrix} \end{bmatrix} = \begin{bmatrix} \begin{bmatrix} g_{2r2r} & g_{2r2i} \\ g_{2i2r} & g_{2i2i} \end{bmatrix} & \cdots & \begin{bmatrix} g_{2rKr} & g_{2rKi} \\ g_{2iKr} & g_{2iKi} \end{bmatrix} \\ \vdots & \ddots & \vdots \\ \begin{bmatrix} g_{Hr2r} & g_{Hr2i} \\ g_{Hi2r} & g_{Hi2i} \end{bmatrix} & \cdots & \begin{bmatrix} g_{HrKr} & g_{HrKi} \\ g_{HiKr} & g_{HiKi} \end{bmatrix} \end{bmatrix} \times \begin{bmatrix} \begin{bmatrix} \Delta I^p_{2r} \\ \Delta I^p_{2i} \end{bmatrix} \\ \vdots \\ \begin{bmatrix} \Delta I^p_{Kr} \\ \Delta I^p_{Ki} \end{bmatrix} \end{bmatrix} \tag{4}$$

where $H$ and $K$ are the maximum harmonic order considered in the matrix derivation; the generic element of the matrix in (4) is a real valued rank 2 tensor evaluated by the following expression:

$$\begin{bmatrix} g_{hrkr} & g_{hrki} \\ g_{hikr} & g_{hiki} \end{bmatrix} = \begin{bmatrix} g^+_{hkr} & -g^+_{hki} \\ g^+_{hki} & g^+_{hkr} \end{bmatrix} + \begin{bmatrix} g^-_{hkr} & g^-_{hki} \\ g^-_{hki} & -g^-_{hkr} \end{bmatrix} \tag{5}$$

where $g^+_{hkr}$ and $g^+_{hki}$ ($g^-_{hkr}$ and $g^-_{hki}$) are the real and imaginary parts of the generic complex element $g^+_{hk}$ ($g^-_{hk}$) of the matrix $\boldsymbol{G}^+$ ($\boldsymbol{G}^-$) in (3), which can be written in a more compact form

$$[\Delta I^s] = [\boldsymbol{G}^{(2)}][\Delta I^p] \tag{6}$$

where $\boldsymbol{G}^{(2)}$ is a matrix whose elements are tensors of rank 2.

If $\boldsymbol{G}^{(2)}$ is invertible, the following relation can be written:

$$[\Delta I^p] = [\boldsymbol{G}^{(2)}]^{-1}[\Delta I^s] = [\boldsymbol{R}^{(2)}][\Delta I^s]. \tag{7}$$

The ratio compensation matrix $\boldsymbol{R}^{(2)}$ in (7) can be used to compensate for the measured secondary current spectrum.

In practice, as $\boldsymbol{R}^{(2)}$ is derived at a specific operating point, the CT should be characterized at several expected operating points and the appropriate compensation matrix selected basing on the observed operating condition. Alternatively, the computational burden can be reduced by considering that as $\boldsymbol{R}^{(2)}$ is a real-valued matrix, it is mathematically possible to obtain a single, averaged matrix from these individual matrices. The error introduced by either approach will depend on the specific CT characteristics and the number of discrete intervals defined.

## III. Measurement Setup

### A. Hardware Description

The block diagram of the setup for CT characterization is shown in Fig. 1. Current generation is obtained through the Fluke 52120A transconductance amplifier (up to three in parallel, each rated up to 120 A, up to 10 kHz), remotely controlled through IEEE 488. It is driven by the NI PXI (PCI eXtension for Instrumentation) 5422 arbitrary waveform generator (AWG) (±12 V, 200 MHz maximum sampling rate, 16 bit, onboard memory 256 MB).

The AWG is housed in a PXI chassis and the 10 MHz PXI clock is used as the reference clock for its high-resolution phase-locked loop circuitry. The generation frequency of the AWG is therefore chosen to be an integer multiple of the generated fundamental frequency.

Another AWG is used to generate a 12.8 MHz clock, which is used as the time base clock for the comparator [22], [23], remotely controlled through a LAN connection. This is based on the NI cDAQ chassis with two different acquisition modules: NI 9239 (±10 V, 24 bit, and 50 kHz) and NI 9238 (±500 mV, 24 bit, and 50 kHz). In this way, generation and acquisition are synchronized.

The current reference value is obtained by means of a set of calibrated current shunts (REF in Fig. 1), Fluke A40B series, 1/0.8, 5/0.8, 20/0.8, and 100/0.8 A/V. They are among the most accurate current shunts, with an input frequency range up to 100 kHz, available on the market, with the best accuracy of some parts per million. The output current of the CT is sensed through a LEM NORMA TRIAX Shunt (SH in Fig. 1), 30/300 A/mV (0.03% up to 100 kHz).

### B. CT Testing Procedure

In order to characterize the CT performance in the presence of distorted signals, an event-based state machine has been developed in LabVIEW. A large choice of signal types may be selected, for example, sinusoidal, fundamental plus a harmonic tone (FH1), fundamental with N harmonics (FHN), and fundamental with an interharmonic (FI1).

Once the signal is generated, the software waits for a variable time interval, depending on the setup configuration, in order to ensure that all of the devices are at the correct operating temperature. Then, the output waveforms of the REF and the CT under test (CT in Fig. 1) are simultaneously sampled and stored in files. The sampling frequency is set to 50 kHz. The samples stored in the files are then postprocessed in the MATLAB environment.

The CT complex frequency response is determined at every frequency component that is generated: as the sampling is synchronous with generation, the phasors of primary and secondary currents are obtained by means of discrete Fourier transform (DFT). Following the calculation of all the phasors, the ratio error and phase error, defined in the following equations, are evaluated for each harmonic component of order $j$:

$$\Delta \mathrm{R}_j = \left( \frac{\mathrm{K}|I_j^s|}{|I_j^p|} - 1 \right) \cdot 100 \tag{8}$$

$$\Delta \varphi_\mathrm{j} = \varphi_\mathrm{j}^\mathrm{s} - \varphi_\mathrm{j}^\mathrm{p} \tag{9}$$

where $K$ is the rated ratio of the CT, $|I_j^p|$ and $\varphi_j^p$ are the amplitude and phase angle of the primary current, and $|I_j^s|$ and $\varphi_j^s$ are the amplitude and phase angle of the secondary current, obtained, respectively, from the output of the reference shunt and the shunt at the CT secondary winding.

In order to evaluate the performance of the proposed compensation technique, the ratio and phase errors are also evaluated with the compensated secondary current

$$\Delta \mathrm{R}_{\mathrm{FCM},j} = \left( \frac{|\tilde{I}_j^p|}{|I_j^p|} - 1 \right) \cdot 100 \tag{10}$$

$$\Delta \varphi_{\mathrm{FCM,j}} = \tilde{\varphi}_\mathrm{j}^\mathrm{p} - \varphi_\mathrm{j}^\mathrm{p} \tag{11}$$

where $|\tilde{I}_j^p|$ and $\tilde{\varphi}_j^p$ are the amplitude and the phase angle of the primary current obtained by compensating the secondary current with the FCM.

### C. Characterization of the Measurement Setup

The evaluation of the equations (8)–(11) requires the knowledge of the complex gain of the CT, i.e., the ratio of the secondary to primary current phasors. Following Fig. 1, the complex gain $G_j^\mathrm{CT}$ of the CT, for the $j$th harmonic component, can be expressed as

$$G_j^\mathrm{CT} = \frac{I_j^s}{I_j^p} = \frac{G_j^\mathrm{REF}}{V_j^\mathrm{REF}} \frac{V_j^\mathrm{SH}}{G_j^\mathrm{SH}} = \frac{V_j^1}{V_j^0} \frac{G_j^0}{G_j^1} \frac{G_j^\mathrm{REF}}{G_j^\mathrm{SH}} \tag{12}$$

where $V_j^\mathrm{REF}$ ($V_j^\mathrm{SH}$), $G_j^0$ ($G_j^1$), and $V_j^0$ ($V_j^1$) are, respectively, the phasor of the voltage at the output of the shunt REF (SH) acquired by channel 0 (channel 1) of the comparator, the complex gain of the channel 0 (channel 1) and the measured phasor by the channel 0 (channel 1). $G_j^\mathrm{REF}$ and $G_j^\mathrm{SH}$ are the complex gains of shunt REF and SH.

Therefore, the measurement of $G_j^\mathrm{CT}$, and thus the measurement of the quantities in (8)–(11) is affected by the systematic errors introduced by the quantities

$$\Delta G_j^\mathrm{COMP} = \frac{G_j^0}{G_j^1} \tag{13}$$

$$\Delta G_j^S = \frac{G_j^\mathrm{REF}}{G_j^\mathrm{SH}} \tag{14}$$

TABLE I

SYSTEMATIC RATIO AND PHASE ERRORS, AND RELATIVE EXPANDED UNCERTAINTY (99%), INTRODUCED BY THE COMPARATOR AT 50 HZ AND 10 KHZ FOR SIGNALS OF 10% OF THE INPUT RANGE

| | 50 Hz | | 10 kHz | |
|---|---|---|---|---|
| | Systematic Error | U (99 %) | Systematic Error | U (99 %) |
| Ratio Error (μV/V) | 2 | 1 | 170 | 15 |
| Phase Error (μrad) | 2 | 3 | 120 | 70 |

which, in turn, have to be measured and compensated. These quantities have been measured by performing tests of type FH1.

$\Delta G_j^{\mathrm{COMP}}$ is linked to the accuracy of the comparator, whose characterization has been extensively discussed in [22]. The systematic ratio and phase errors, and the relative expanded uncertainty (99% confidence level), introduced by the comparator at 50 Hz and 10 kHz, for input signals equal to 10% (i.e., 0.7 V) of the full-scale range, are summarized in Table I.

$\Delta G_j^S$ represents the mismatch between the frequency responses of the primary (reference) and the secondary shunts of the CT. As different reference shunts are used, different $\Delta G_j^S$ have been evaluated for each, using the same measurement setup shown in Fig. 1 (excluding the CT under test and making the primary current flow into both REF and SH shunts).

Another important feature of a calibration setup for instrument transformers is the accuracy of the generated current value. The accuracy of the generated current depends both on the stability and on the repeatability of the AWG and of the amplifier. Specific tests (of type FH1) have been performed to evaluate the stability and the repeatability of the generated current. The stability, evaluated as the standard deviation of the amplitude and phase of the current during a specific test, was very good, lower than five parts per million. However, the repeatability, evaluated as the standard deviation of amplitude and phase of current generated over several repetitions of each FH1 test, was in the order of 0.05% and was considered not acceptable for the application at hand.

Therefore, in order to improve the repeatability of the generated current, a closed loop generation has been used: for each test, the desired waveform is generated and acquired. If the amplitude and phase of the generated tones differ from the desired values, the waveform is regenerated until both values are within 10 $\mu$A/A and 10 $\mu$rad. In this way, a very precise and accurate signal is obtained up to 10 kHz. In particular, the gain and phase errors of the generation system are below 10 $\mu$A/A and 10 $\mu$rad up to 10 kHz; the expanded uncertainties (95% confidence level) are 8 $\mu$A/A and 11 $\mu$rad at 47 Hz and 92 $\mu$A/A and 2.2 mrad at 10 kHz.

### D. Current Transformers Under Test

The previously described system has been used to characterize the behavior of two commercial CTs. The first CT, named CT1, is a window type 100/5 A/A CT, with a rated ratio of 20, accuracy class of 1 and rated burden of 3 VA.

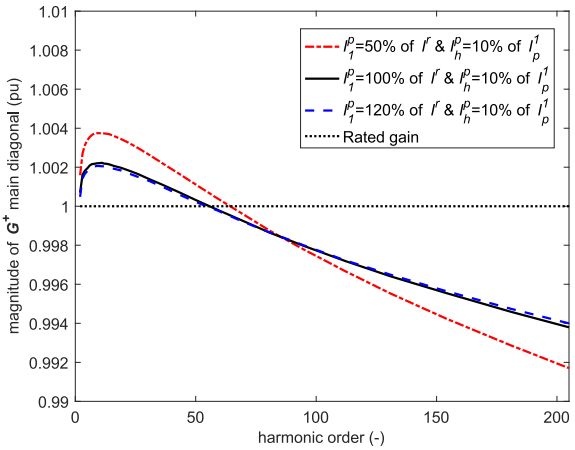


Fig. 2. CT1: Values of the main diagonal elements of the matrix $\boldsymbol{G}^+$ in p.u. of the rated ratio of the CT.

The second CT, named CT2, is a wound 10/5 A/A CT, with a rated ratio of 2, accuracy class of 0.5, and rated burden of 5 VA. For both of the CTs, the operating frequency is 50/60 Hz. For CT1, one additional primary turn is used in order to increase the equivalent measured primary current. In this way, CT1 becomes a 50/5 A/A CT, with a ratio equal to 10. Regarding the burden, all tests have been performed with only shunt SH connected to the secondary terminals of the CTs; as it has a resistance of 10 mΩ, it corresponds to a burden of 0.25 VA, i.e., 8% burden for CT1 and 5% for CT2.

## IV. COMPENSATION MATRIX DERIVATION

The compensation matrix calculation process begins with the derivation of the gain matrices $\boldsymbol{G}^+$ and $\boldsymbol{G}^-$ (3) and then the ratio compensation matrix $\boldsymbol{R}^{(2)}$ is computed using (4)–(7).

Various tests of type FH1 have been performed on both CTs. Three amplitudes, 120%, 100%, and 50%, of the CT's rated value $I^r$ and zero phase angle have been used for the fundamental tone. For the fundamental frequency, a value of 47 Hz was chosen to avoid interference with the power system frequency. An amplitude of 10% of the CT's rated value, 30 log-spaced frequencies from 2nd to 213th order (i.e., about 10 kHz) and 13 phase angles from 0 to $2\pi$ have been used for the sweeping harmonic tone. For each test waveform, a sampling frequency of 50 kHz was used and 50 000 points acquired (i.e., 1 s). Measurements with each test waveform were repeated ten times.

### A. Current Transformer CT1

Fig. 2 shows the magnitudes of the main diagonal elements of the gain matrix $\boldsymbol{G}^+$ in (3) for CT1, normalized with the gain measured at the fundamental frequency (dotted black line), versus the harmonic order, for the three fundamental magnitudes analyzed with a superimposed harmonic of 10%. The maximum deviation between the three operating points (∼0.2%) is about one order of magnitude lower than the declared accuracy class limit. The two curves corresponding to $I_1^p = 100\%$ and 120% of $I^r$ are almost coincident. It is also possible to observe that due to the effect of stray parameters

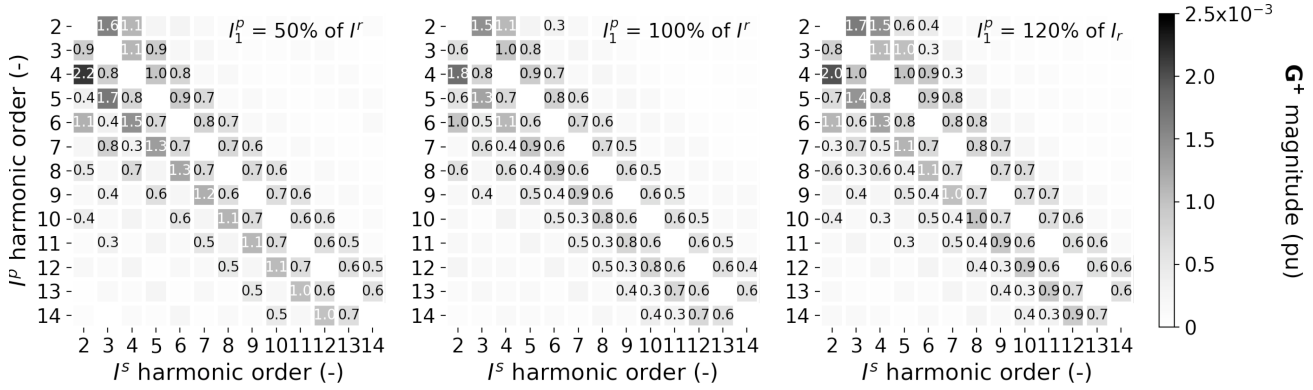


Fig. 3. CT1: Values of the off-diagonal elements of matrix $\boldsymbol{G}^+$ in p.u. of the rated ratio of the CT versus the harmonic order for the three fundamental currents considered.

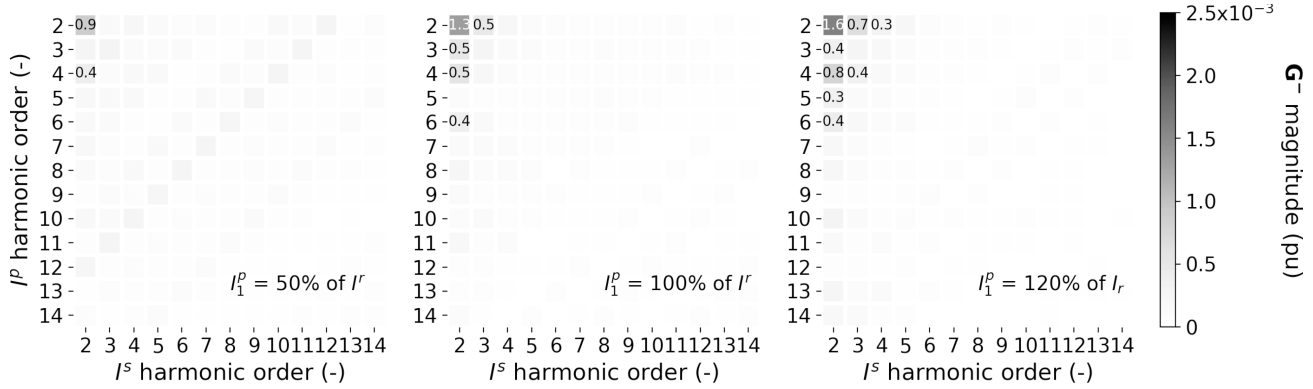


Fig. 4. CT1: Values of the matrix $\boldsymbol{G}^-$ in p.u. of the rated ratio of the CT versus the harmonic order for the three fundamental currents considered.

(leakage inductance and coupling capacitances between the turns), when the harmonic order increases (above ~10 kHz), the gain trend is likely to exit from the declared accuracy class.

Fig. 3 shows the magnitudes of the off-diagonal elements of the gain matrix $\boldsymbol{G}^+$ that takes into account the cross coupling between harmonics of the primary current with harmonics of the secondary current of different orders (cross-coupling gains) due to the nonlinearities present. The harmonic order is limited to 14, as the values beyond this range are of such small magnitude that they have little effect on the CT response.

Fig. 4 shows the magnitudes of the elements (diagonal and off-diagonal) of the gain matrix $\boldsymbol{G}^-$ that takes into account the phase angle dependence between harmonics of different orders due to the nonlinearities present (phase-dependent gains). Values greater than 0.3 are marked in the matrix plots.

From Figs. 3 and 4, it is possible to observe the following.

1) The main coupling is between the adjacent harmonics along the matrix diagonals; this coupling decreases with frequency (Fig. 3).
2) The coupling for $I_1^p = 50\%$ is slightly higher but there is not a large difference between the three working points.
3) The values of such gains (Fig. 3) are about three orders of magnitude lower than those of the main diagonal (Fig. 2), demonstrating an overall linear behavior of the CT.
4) The phase dependence (Fig. 4) is almost negligible, as the elements of the matrix $\boldsymbol{G}^-$ are about one order of magnitude lower than those of $\boldsymbol{G}^+$, except for the second on itself (primary versus secondary) and on the third and fourth harmonics.

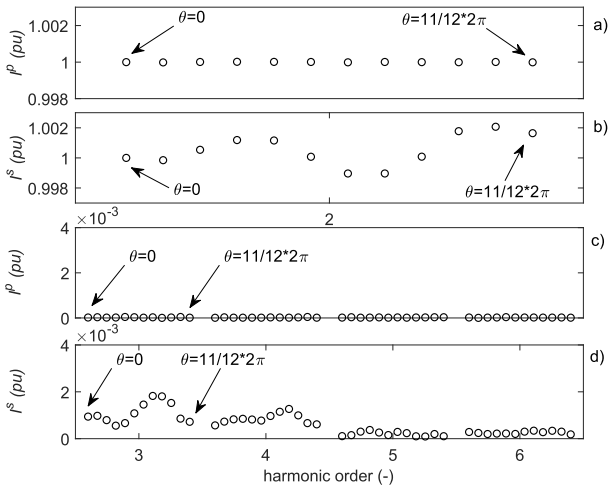


Fig. 5. CT1: Exemplar magnitudes first five harmonic orders of the secondary current for the 12 phase angle considered in the tests.

The cross coupling and the phase dependence modeled by the matrices $\boldsymbol{G}^+$ and $\boldsymbol{G}^-$ can be better appreciated in Fig. 5, which reports the magnitudes of the first five harmonic orders of the primary $I^p$ and secondary current $I^s$ observed for the 12 phase angles considered during an FH1 test with 100% fundamental tone and 10% second harmonic.

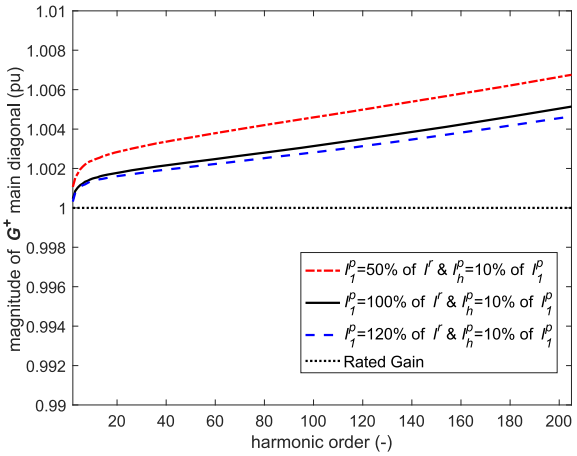


Fig. 6. CT2: Values of the main diagonal elements of the matrix $\boldsymbol{G}^+$ in p.u. of the rated ratio of the CT.

When the (approximately) constant second-order harmonic is superimposed on the primary side fundamental component $I^p$ [Fig. 5(a)], the other harmonics are almost nil [Fig. 5(c)], demonstrating the very good performance of the generation system.

However, the second-order harmonic on the secondary side $I^s$ [Fig. 5(b)] is shifted up by $1 \cdot 10^{-3}$ p.u. (c.f. the gain on Fig. 2 at the second-harmonic order) and oscillates with an amplitude of about $1 \cdot 10^{-3}$ p.u. due to the phase angle dependence on itself ($1.2 \cdot 10^{-3}$ p.u. in the corresponding square of Fig. 4). The cross-coupling effect is evident around the third–fifth harmonics [Fig. 5(d)], which show amplitudes comparable to the corresponding gain values of Fig. 3, with oscillations with amplitudes comparable to the corresponding gain values of Fig. 4.

### B. Current Transformer CT2

Figs. 6, 7, and 8 are equivalent to Figs. 2, 3, and 4. From Fig. 6, it is possible to observe that the values of the main diagonal elements of the matrix $\mathbf{G}^+$ increase with frequency, showing a possible resonance at frequencies over 10 kHz. Moreover, for a primary current of 50% of the rated current, the gain exits from the accuracy class (i.e., it exceeds 1.005 p.u.) around the 120th harmonic order (i.e., around 5.7 kHz). From Fig. 8, it is evident that CT2 exhibits a similar trend to CT1, i.e., the main coupling is between the adjacent harmonics along the matrix diagonals, this coupling decreases with frequency and the values obtained for the three operating points are similar, despite the difference in the main diagonal response. However, the magnitudes of the matrix elements are smaller than those of CT1; comparing Figs. 3 and 7, it is seen that values in Fig. 7 are almost half the magnitude of those in Fig. 3. Concerning the phase dependence (Fig. 8), it is evident that it is almost negligible, except for the second harmonic on itself.

## V. Verification by Means of Random Signals

An experimental case study using 100 synthetic waveforms applied to the CTs was used to assess the performance of the compensation matrixes derived. The waveforms consist of a fundamental tone $I^p = 100\%$ of $I^r$ and harmonics across the entire frequency range considered; however, the total harmonic distortion (THD) is fixed at 10% and the harmonic magnitudes and phase are randomly allocated based on this constraint.

Three different ratio and phase errors have been compared: a) those calculated with (10) and (11), i.e., using the FCM approach; b) those calculated with (8) and (9) i.e., with a constant ratio (CR) measured at fundamental frequency; and c) those calculated with (10) and (11) but using only the inverse of the elements of the main diagonal of $\boldsymbol{G}^+$ ($\mathrm{DR}^+$), of the derived matrix, to compensate the secondary current. The $\mathrm{DR}^+$ method is equivalent to using a linear model for the CT, which makes use of a complex gain variable with frequency [see Figs. 2 and 6], to compensate the secondary current.

### A. Current Transformer CT1

The results in Figs. 9 and 10 show the ratio and phase errors [see (8)–(11)] versus the harmonic order for CT1 using the three different methods considered by means of boxplots. For each box, the central mark is the median, the edges of the box are the 25th and 75th percentiles, and the whiskers extend to the most extreme data points ($\pm 2.7\sigma$ and 99.3% coverage if the data are normally distributed) not considering outliers. The declared accuracy class borders ($\pm 1\%$ and $\pm 1.8$ crad) are also marked.

It is possible to observe the following.

1) The proposed FCM method accurately compensates the nonlinearities of the CT for the entire considered frequency range, maintaining both ratio and phase errors within one accuracy class below the declared value.
2) The CR and $\mathrm{DR}^+$ approaches, as they assume a linear model for the CT, are not able to compensate the nonlinearities, which are responsible for the very high amplitude of the whiskers, especially at low frequencies.
3) The ratio error of the CR approach is outside the accuracy class for the first four harmonics (around $\pm 5\%$ at the third harmonic) and reaches the lower boundary of the accuracy class at the end of the frequency range considered.
4) The phase error of the CR approach is outside the accuracy class for the first two harmonics and also exits the lower border boundary around the 95th harmonic (4.5 kHz).
5) The ratio and phase errors of the $\mathrm{DR}^+$ approach are similar to those of the CR approach but, after the fifth harmonic, they remain within the declared accuracy class range as, unlike the CR method, the $\mathrm{DR}^+$ approach evaluates the ratio and phase errors using a complex gain variable with frequency.

### B. Current Transformer CT2

Figs. 11 and 12 are equivalent to Figs. 9 and 10 but for CT2. The declared accuracy class borders ($\pm 0.5\%$ and $\pm 0.9$ crad) are also marked. It is possible to observe the following.

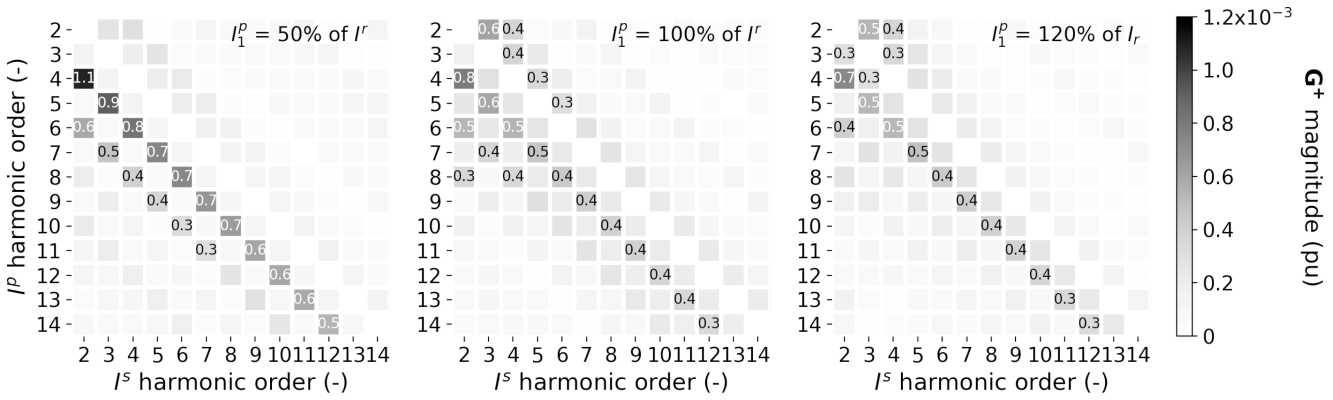


Fig. 7. CT2: Values of the off-diagonal elements of the matrix $\boldsymbol{G}^+$ in p.u. of the rated ratio of the CT versus the harmonic order for the three fundamental currents considered.

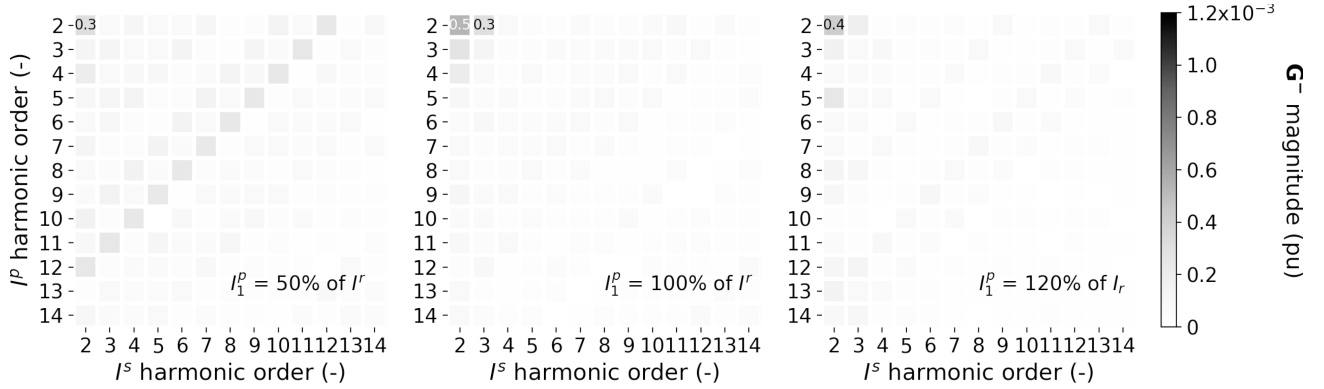


Fig. 8. CT2: Values of the matrix $\boldsymbol{G}^-$ in p.u. of the rated ratio of the CT versus the harmonic order for the three fundamental currents considered.

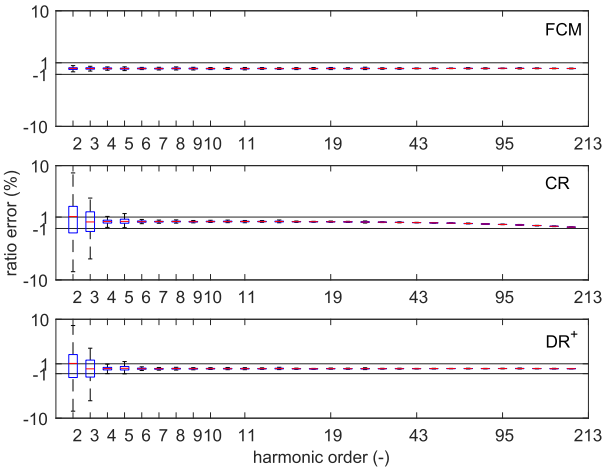


Fig. 9. CT1: Ratio error evaluated at rated current $I^r$ with FCM, CR, and DR$^+$ versus the harmonic order.

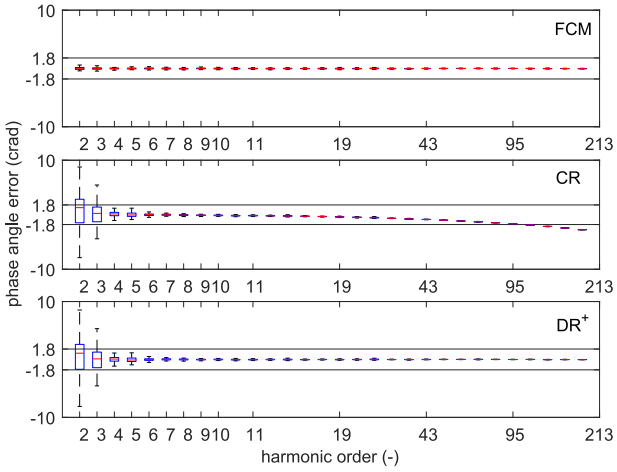


Fig. 10. CT1: Phase angle error evaluated at rated current $I^r$ with FCM, CR, and DR$^+$ versus the harmonic order.

1) Again, the FCM method allows the CT to remain in the declared accuracy class for the entire frequency range of interest.
2) The CR and DR$^+$ approaches are not able to compensate the CT nonlinearities.
3) The first two harmonics are largely outside from the declared class limit for both the CR and DR$^+$ approaches, with values up to $\pm 3.5\%$ ratio error and $\pm 3.5$ crad phase error observed for the second and third harmonics.
4) The CR approach also exits from the class accuracy at the highest frequency, i.e., 10 kHz, analyzed in this paper; however, unlike CT1, the phase error of the higher order harmonics is maintained within the accuracy class.

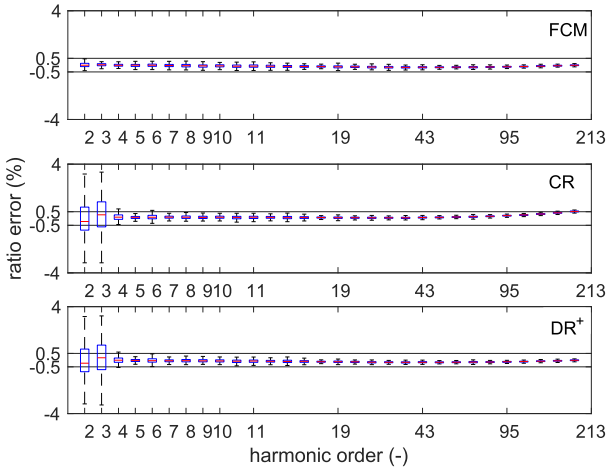


Fig. 11. CT2: Ratio error evaluated at rated current $I^r$ with FCM, CR, and DR$^+$ versus the harmonic order.

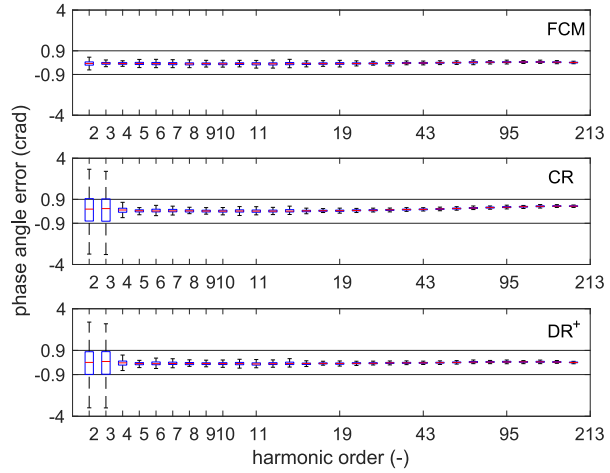


Fig. 12. CT2: Phase angle error evaluated at rated current $I^r$ with FCM, CR, and DR$^+$ versus the harmonic order.

5) Similar to comment 5) in Section V.A, DR$^+$ performs better than CR, allowing the ratio and phase error to remain within the declared accuracy class for the frequency range of interest, beyond the fourth harmonic order.

## VI. Conclusion

This paper has presented a new approach for the compensation of the nonlinearities of a CT by modeling its complex ratio using a frequency domain model based on the FCM approach and tensor linearization.

An accurate measurement setup has been built to characterize CTs performance in distorted conditions up to 10 kHz. Two commercial CTs belonging to two different accuracy classes have been characterized and modeled.

The proposed compensation technique has been applied to the two CTs using a set of 100 random signals.

The main outcomes of this paper are as follows.

1) It provides a methodology to test a CT and to analyze its nonlinearity, quantifying the cross-coupling effects and the phase dependence between primary and secondary current harmonics of different orders.
2) It proposes a new compensation technique that allows a CT to maintain its accuracy class, or to improve it, for every kind of distorted primary current and in a wide frequency range, up to several kilohertz.
3) The computational load of the proposed approach is low since it consists of simple summations and multiplications between real numbers.
4) This compensation technique can be easily implemented even on low-cost power and power quality measuring instruments, typically characterized by low computational performance, thus improving their accuracy in a wide frequency range.
5) As the proposed methodology is fully digital, it can be easily implemented in IEDs (Intelligent Electronic Devices, e.g. merging units and digital relays) [24], [25], which are key components of the new digital substations, to improve the performance of both measuring, as well as protection devices.

## Acknowledgment

The paper was prepared at the SUN-EMC Laboratory, University of Campania "Luigi Vanvitelli," Aversa (CE), Italy.

## References

[1] A. Cataliotti, D. Di Cara, A. E. Emanuel, and S. Nuccio, "Current transformers effects on the measurement of harmonic active power in LV and MV networks," *IEEE Trans. Power Del.*, vol. 26, no. 1, pp. 360–368, Jan. 2011.

[2] A. Cataliotti, D. Di Cara, A. E. Emanuel, and S. Nuccio, "A novel approach to current transformer characterization in the presence of harmonic distortion," *IEEE Trans. Instrum. Meas.*, vol. 58, no. 5, pp. 1446–1453, May 2009.

[3] M. Faifer, C. Laurano, R. Ottoboni, S. Toscani, and M. Zanoni, "Characterization of voltage instrument transformers under nonsinusoidal conditions based on the best linear approximation," *IEEE Trans. Instrum. Meas.*, vol. 67, no. 10, pp. 2392–2400, Oct. 2018.

[4] T. Lei *et al.*, "Behavior of voltage transformers under distorted conditions," in *Proc. IEEE Int. Instrum. Meas. Technol. Conf.*, May 2016, pp. 1–6.

[5] M. Faifer, C. Laurano, R. Ottoboni, S. Toscani, and M. Zanoni, "A simple method for compensating the harmonic distortion introduced by voltage transformers," in *Proc. 9th Int. Workshop Appl. Meas. Power Syst. (AMPS)*, Sep. 2018, pp. 1–6.

[6] A. Cataliotti *et al.*, "Compensation of nonlinearity of voltage and current instrument transformers," *IEEE Trans. Instrum. Meas.*, to be published.

[7] N. Locci and C. Muscas, "Hysteresis and eddy currents compensation in current transformers," *IEEE Trans. Power Del.*, vol. 16, no. 2, pp. 154–159, Apr. 2001.

[8] M. Zou, W. Sima, M. Yang, L. Li, Q. Yang, and P. Sun, "Improved low-frequency transformer model based on Jiles-Atherton hysteresis theory," *IET Gener., Transmiss. Distrib.*, vol. 11, no. 4, pp. 915–923, 2017.

[9] X. Wang, D. W. P. Thomas, M. Sumner, J. Paul, and S. H. L. Cabral, "Characteristics of Jiles-Therton model parameters and their application to transformer inrush current simulation," *IEEE Trans. Magn.*, vol. 44, no. 3, pp. 340–345, Mar. 2008.

[10] J. Arrillaga, B. C. Smith, N. R. Watson, and A. R. Wood, *Power System Harmonic Analysis*. Hoboken, NJ, USA: Wiley, 1997.

[11] B. C. Smith, N. R. Watson, A. R. Wood, and J. Arrillaga, "Harmonic tensor linearisation of HVDC converters," *IEEE Trans. Power Del.*, vol. 13, no. 4, pp. 1244–1250, Oct. 1998.

[12] Y. Sun, G. Zhang, W. Xu, and J. G. Mayordomo, "A harmonically coupled admittance matrix model for AC/DC converters," *IEEE Trans. Power Syst.*, vol. 22, no. 4, pp. 1574–1582, Nov. 2007.

[13] R. Carbone, A. L. Schiavo, P. Marino, and A. Testa, "Frequency coupling matrixes for multi stage conversion system analysis," *Eur. Trans. Elect. Power*, vol. 12, no. 1, pp. 17–24, Jan./Feb. 2002.

[14] P. W. Lehn and K. L. Lian, "Frequency coupling matrix of a voltage-source converter derived from piecewise linear differential equations," *IEEE Trans. Power Del.*, vol. 22, no. 3, pp. 1603–1612, Jul. 2007.
[15] L. Frater, "Light flicker and harmonic modelling of electrical lighting," Ph.D. dissertation, Dept. Elect. Comput. Eng., Univ. Canterbury, Christchurch, New Zealand, 2015.
[16] M. F. Romero, L. E. Gallego, S. Müller, and J. Meyer, "Characterization of non-linear household loads for frequency domain modeling," *Ing. Invest.*, vol. 35, pp. 65–72, Dec. 2015.
[17] M. Fauri, "Harmonic modelling of non-linear load by means of crossed frequency admittance matrix," *IEEE Trans. Power Syst.*, vol. 12, no. 4, pp. 1632–1638, Nov. 1997.
[18] R. Langella *et al.*, "On the use of Fourier descriptors for the assessment of frequency coupling matrices of power electronic devices," in *Proc. 18th Int. Conf. Harmon. Qual. Power (ICHQP)*, Ljubljana, Slovenia, May 2018, pp. 1–6.
[19] J. E. Caicedo, A. A. Romero, H. C. Zini, R. Langella, J. Meyer, and N. R. Watson, "Impact of reference conditions on the frequency coupling matrix of a plug-in electric vehicle charger," in *Proc. 18th Int. Conf. Harmon. Qual. Power (ICHQP)*, Ljubljana, Slovenia, May 2018, pp. 1–6.
[20] D. Gallo, R. Langella, M. Luiso, A. Testa, and N. R. Watson, "A new test procedure to measure power electronic devices' frequency coupling admittance," *IEEE Trans. Instrum. Meas.*, vol. 67, no. 10, pp. 2401–2409, Oct. 2018.
[21] A. J. Collin, A. D. Femine, D. Gallo, R. Langella, and M. Luisa, "Compensation of current transformers' non-linearities by means of frequency coupling matrices," in *Proc. IEEE 9th Int. Workshop Appl. Meas. Power Syst. (AMPS)*, Sep. 2018, pp. 1–6.
[22] G. Crotti, D. Gallo, D. Giordano, C. Landi, and M. Luiso, "Industrial comparator for smart grid sensor calibration," *IEEE Sensors J.*, vol. 17, no. 23, pp. 7784–7793, Dec. 2017.
[23] G. Crotti *et al.*, "Calibration of current transformers in distorted conditions," *J. Phys., Conf. Ser.*, vol. 1065, no. 5, 2018, Art. no. 052033. doi: 10.1088/1742-6596/1065/5/052033.
[24] *Communication Networks and Systems for Power Utility Automation - Part 1: Introduction and Overview*, document ITU 61850-1, 2013.
[25] S. D. Prete, A. D. Femine, D. Gallo, C. Landi, and M. Luiso, "Implementation of a distributed stand alone merging unit," *J. Phys., Conf. Ser.*, vol. 1065, no. 5, 2018, Art. no. 052042.

**Adam J. Collin** (S'10–M'12) was born in Edinburgh, Scotland, in 1985. He received the B.Eng. degree in electrical and electronic engineering from the University of Edinburgh, in 2007, the M.Sc. degree in renewable energy and distributed generation from Heriot-Watt University, in 2008 and the Ph.D. degree from the University of Edinburgh, in 2013.

He is currently a Researcher with the University of Campania "Luigi Vanvitelli," Aversa, Italy. His current research interests include power system harmonics, load modeling, and distribution system analysis.

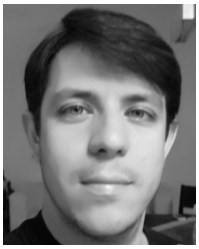

**Antonio Delle Femine** (S'18–M'19) was born in Caserta, Italy, in 1980. He received the M.Sc. degree (*summa cum laude)* in electronic engineering and the Ph.D. degree in electrical energy conversion from the University of Campania "Luigi Vanvitelli," Aversa (CE), Italy, in 2005 and 2008, respectively.

From 2008 to 2017, he was a Freelancer with many national and international companies. He worked as Software Engineer, Senior Embedded Firmware Engineer, Hardware Engineer, and Project Manager. He was involved in the design of many products for both industrial and consumer electronics: fleet monitoring systems, thermal printers, electronic scales and cash registers, distributed monitoring systems for photovoltaic plants, Hi-Fi radios and home appliances, automatic end-of-line testing systems, augmented reality devices, and radioactivity measurement instrumentation (in collaboration with national institute of nuclear physics, INFN). In 2018, he joined the University of Campania "Luigi Vanvitelli" as a Researcher. His current research interests include the power measurement theory, the design, implementation and characterization of digital-measurement instrumentation of automatic measurement systems, and the radioactivity measurements.

Dr. Femine is a member of the IEEE Instrumentation and Measurement Society.

**Daniele Gallo** (S'00–M'04) was born in Santa Maria C. V. (CE), Italy, in 1974. He received the Laurea degree in electronic engineering and the Ph.D. degree in electrical energy conversion from University of Campania "Luigi Vanvitelli," Aversa (CE), Italy, in 1999 and 2003, respectively.

He is currently an Associate Professor with the University of Campania "Luigi Vanvitelli." He has authored or coauthored more than 130 papers published in books, international scientific journals, and conference proceedings. His current research interests include design, implementation, and characterization of measurement systems for electrical power system, power quality issues, power and energy measurement in nonsinusoidal conditions, design and implementation of smart meter for smart grid application, and electrical transducer characterization.

**Roberto Langella** (S'00–M'01–SM'10) was born in Naples, Italy, in 1972. He received the Laurea degree in electrical engineering from the University of Naples, Naples, Italy, in 1996, and the Ph.D. degree in electrical energy conversion from the University of Campania L. Vanvitelli, Aversa, Italy, in 2000.

He is currently a Full Professor of electrical power systems with the University of Campania L. Vanvitelli. He is a Senior Member of the IEEE Power Engineering Society, Vice Chair of the IEEE PES Italy Section, and Chair of the IEEE PES Task Force on Harmonic Modeling, Simulation, and Assessment.

**Mario Luiso** (S'07–M'08) was born in Naples, Italy, in 1981. He received the Laurea degree (*summa cum laude*) in electronic engineering and the Ph.D. degree in electrical energy conversion from the University of Campania "Luigi Vanvitelli," Aversa (CE), Italy, in 2005 and 2007, respectively.

He currently is an Associate Professor with the Department of Engineering, University of Campania "Luigi Vanvitelli." He has authored or co-authored more than 150 papers published in books, international scientific journals, and conference proceedings. His current research interests include the development of innovative methods, sensors and instrumentation for power system measurements, in particular power quality, calibration of instrument transformers, phasor measurement units, and smart meters.

Dr. Luiso is a member of the IEEE Instrumentation and Measurement Society.